Solar Panel Simulation for Testing of Nanosatellite Power Systems

Gustav M. Pettersson[a,*], Malte Gruber[a], Theodor-Adrian Stana[b], Sven Grahn[c,**], Christer Fuglesang[c]

[a] *School of Engineering Sciences, KTH Royal Institute of Technology, Stockholm 100 44, Sweden*
[b] *Department of Particle and Astroparticle Physics, KTH Royal Institute of Technology, Stockholm 114 21, Sweden*
[c] *KTH Space Center, KTH Royal Institute of Technology, Stockholm 114 28, Sweden*

Abstract

Sufficient testing of the power generation subsystem on nanosatellites (e.g. CubeSats) is often forgone due to the difficulties and cost involved in recreating the orbital solar environment. In this paper, a novel and accessible method to test the power system of a solar panel powered nanosatellite is presented. Hardware is designed and prototyped to apply several independent and arbitrary solar panel current vs. voltage curves in real-time to the satellite. This simulated output is wired into the nanosatellite harness in place of the solar panels and allows all systems downstream of the solar panel connections to be tested in a realistic setting. To accompany this, a process to convert data of the illumination of the solar cells of the satellite into characteristic solar panel curves is shown. Performance measurements of the system are provided, as well as test results when attached to a CubeSat. These measurements show that the system reproduces a realistic and low-noise input to the satellite as desired. Hardware and software are released freely under an Open Source licence.

Keywords: CubeSat, Hardware-in-the-Loop, Power System, Testing, Solar Array Interface, Open Source

1. Introduction

Realistic ground testing of satellite power systems is expensive due to difficulties in reproducing the solar environment in orbit. With the recent increased demand for nanosatellites, such as CubeSats, in which the development cost has decreased dramatically, there is often little room in the budget for such testing. Since the power system is one of the most important subsystems on a satellite, there is a need for alternative testing methods.

In this paper, an accessible and practical method to test the power system of nanosatellites is described. The method is based on simulating the expected electrical behaviour of the solar panels and using computer controlled hardware to emulate these at the power system inputs. It is assumed that detailed simulations developed for the optimisation of the solar panel configurations, e.g. [1], have been conducted and the resulting individual cell illumination in orbit is available. Intuitive and fast methods which use this data to calculate the combined solar panel behaviour of the satellite are presented. The methods are necessitated by the growing number of deployable structures (such as solar panels, booms, and antennae) on nanosatellites. These structures can partially shade solar cells on the satellite, creating complex solar panel curves and degrading the overall power output [2].

A computer controlled hardware simulation circuit, implemented on a small Printed Circuit Board (PCB), which can provide arbitrary current vs. voltage curves is described and connected to the satellite power system. The programmed solar panel curves in the hardware are updated in real-time based on the simulation results. With this developed system, every component of the satellite downstream from the solar panel connections can be tested and verified in the lab before launch, during realistic orbit conditions and with known inputs. The system described in this paper is developed for use in nanosatellite testing; each independent output channel is capable of supplying approximately 25 W.

The hardware and software developed and presented in this paper has been released under an Open Source licence and is free for anyone to use, see the project GitHub website [3].

1.1. Paper overview

An overview of the simulation system is shown in Figure 1. It is assumed that the illumination levels for each cell on the satellite is known from e.g. previous simulations of the satellite. One description of how such a system can be developed is given in [1]. Section 2 details how this data is used to model the IV curve of each individual cell, and how these interact to give the complete IV curve present at the input to the satellite power system. Section 3 describes the hardware design of the simulator system. Section 4 discusses how these two developments are used together to

*Corresponding author
**Principal corresponding author
Email addresses: gupet@kth.se (Gustav M. Pettersson), malteg@kth.se (Malte Gruber), stana@kth.se (Theodor-Adrian Stana), sveng@kth.se (Sven Grahn), cfug@kth.se (Christer Fuglesang)

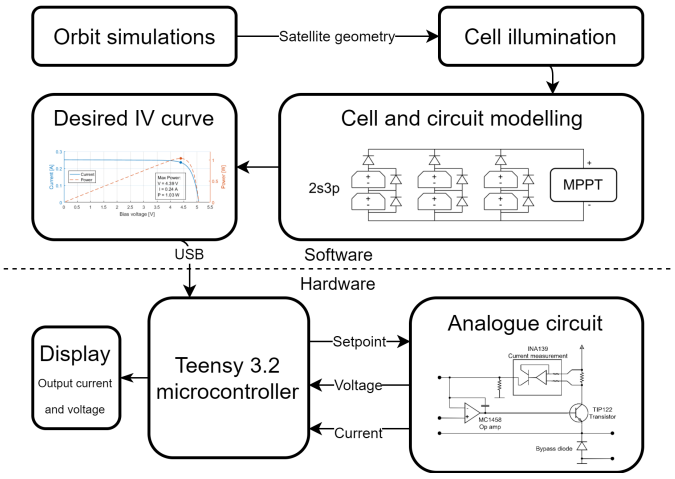

Figure 1: Flowchart overview of the system. The first two steps are not considered in this paper. Sections 2 and 3 concern the parts labelled software and hardware respectively.

provide real-time updating and presents a demonstration of three simulators used together to simulate and verify a full orbit.

1.2. Photovoltaic systems for nanosatellites

Most recent nanosatellites launched use solar cells to generate power in orbit for experiments and subsystems to function [4]. As the complexity of missions carried out on nanosatellites has increased these solar cell arrays have grown to often include deployable panels with a large number of total cells to provide adequate power. Solar cell systems do not act like a typical power supply, where the output voltage is fixed and the maximum current is limited. Instead, they present a current vs. voltage (IV) curve dependent on several factors, most importantly the illumination. This curve must be actively exploited by applying a voltage across the cells to generate power. A Solar Array Interface (SAI) which drives the voltage across each panel is a vital part of any satellite. These come in several flavours, ranging from simple Direct Energy Transfer (DET) systems in which the panels are connected directly to the battery voltage, to Maximum Power Point Tracking (MPPT) systems in which the voltage is actively controlled to always present an optimal load to the solar array, and generate more power [5]. As the solar conditions present on different solar panels and cells differ, it is necessary to have several independent MPPTs on-board for optimal tracking. Typical MPPT based SAIs for nanosatellites provide at least three independent inputs [6], such that each illuminated face may be optimised individually.

1.3. Related previous work

The design of hardware solar panel simulators has been studied repeatedly in the case of grid power generation. The simplest design is formed by a circuit that amplifies the IV curve of a photodiode to the scale desired, but only provides limited control of the shape of the IV curve [7]. A more refined analogue approach was shown in [8] where a complex control circuit was developed that could mimic real panels to a much closer degree. More recent approaches employ switching DC-DC converters that are controlled digitally via an FPGA [9] or microcontroller [10] where an arbitrary IV curve can be programmed via a lookup-table (LUT) to match any desired panel characteristic. Commercial systems for solar array simulation are also available. These typically provide high power (often $> 500\,\mathrm{W}$) per channel [11] and are not suited for nanosatellite testing where several independent outputs of low power ($\leq 20\,\mathrm{W}$) are needed.

The issue has also been studied previously in the nanosatellite regime. A switching DC-DC architecture was applied in [12] but shows poor accuracy and noise. A fundamentally different approach was taken in [13], where instead of using circuits to simulate the output of panels, the solar spectrum was emulated using a combination of Xenon lamps and LEDs. This has a useful application in testing the full chain of equipment from a cell level but is limited in that the individual cell illumination cannot be controlled and it is difficult to illuminate several panels simultaneously.

Methods have been developed to predict and optimise the power system design of nanosatellites [1]. These provide illumination data on a per-cell basis for real orbits. This information is used as input to the hardware simulators for orbit-realistic real-time tests.

1.4. Design criteria

The hardware is designed to provide several fully independent outputs that are powerful enough to simulate two 3U CubeSat solar panels connected in parallel.[1] These outputs are floating, i.e. isolated from the controlling computer and mains power supply, and provided by a small PCB which is practical to implement in the lab. The outputs can be combined in series or parallel if a higher power is necessary. An arbitrary IV curve can be applied to each of the outputs to simulate any state of the solar panels. The hardware is designed with a bandwidth much higher than the frequency typical SAI updates with and with low output noise. The output is not interrupted while a new IV curve is programmed, allowing for real-time updating.

The software system is designed to accurately and intuitively calculate the IV curves that need to be applied to the hardware. This software is not necessary to run the hardware. Instead, simple IV curves (e.g. of static output) can be applied to the system which still would provide useful testing conditions for the satellite. For a reader interested in only this, Section 2 may be skipped.

[1] In practice this means 16 cells of circa 1 W each.

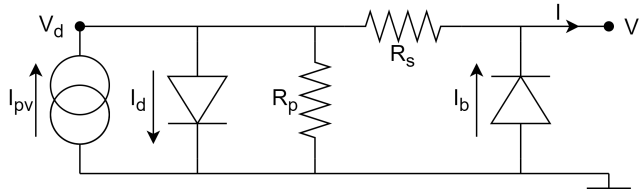

Figure 2: Equivalent circuit of solar cell with bypass diode.

2. Software for IV curve generation

2.1. Photovoltaic cell model

The classic single diode model of a solar cell with parasitic resistances is used in the simulations. The model is shown in Figure 2 where a bypass diode is included. Each component has parameters associated with it which must be matched to the actual cells used in the satellite for good results. From left to right the components and their parameters are:

1. Constant current source (generated current I_{pv})
2. Cell diode (effective thermal voltage V_d^t and saturation current I_d^{sat})
3. Cell shunt resistance (resistance R_p)
4. Cell series resistance (resistance R_s)
5. Bypass diode (effective thermal voltage V_b^t and saturation current I_b^{sat})

Methods for extracting these parameters from measurements is an active area of research, see e.g. [14], and beyond the scope of this paper. For this circuit, the current at a given voltage can be written as [15]:

$$\begin{aligned} I(V) &= \frac{R_p(I_{pv} + I_d^{sat}) - V}{R_p + R_s} - \frac{V_d^t}{R_s} W(\theta(V)) \\ &\quad + I_b^{sat}\left(\exp\left(-V/V_b^t\right) - 1\right) \qquad (1) \\ \theta(V) &= \frac{R_s R_p I_d^{sat}}{V_d^t(R_s + R_p)} \exp\left(\frac{R_p(R_s I_{pv} + R_s I_d^{sat} + V)}{V_d^t(R_s + R_p)}\right) \end{aligned}$$

Where $W(\theta)$ is the Lambert W function,[2] which is defined as the inverse of the following function:

$$\theta = W(\theta) e^{W(\theta)} \qquad (2)$$

By assuming $R_s \ll R_p$ and $I_d^{sat} \ll I_{pv}$ Equation 1 is simplified to:

$$\begin{aligned} I(V) &= I_{pv} - \frac{V}{R_p} - \frac{V_d^t}{R_s} W(\theta(V)) \\ &\quad + I_b^{sat}\left(\exp\left(-V/V_b^t\right) - 1\right) \qquad (3) \\ \theta(V) &= \frac{R_s I_d^{sat}}{V_d^t} \exp\left(\frac{R_s I_{pv} + V}{V_d^t}\right) \end{aligned}$$

[2]The largest value θ will take is approximately $R_s I_{pv}/V_d^t$. Normally this is a small (< 1) number, thus the Lambert W function may be replaced with an approximation which is faster to evaluate.

The model used in these simulations is a practical simplification. In space applications, multi-junction solar cells are common. These consist of a stack of several solar cell junctions optimised for different wavelength bands, internally connected in series. More complex circuit models which explicitly contain this have been developed [16]. However, comparisons of these models by fitting parameters to measured data of multi-junction solar cells show that high accuracy can be reproduced even with the simpler single diode model [17].

The circuit simulations employed in this paper are limited to a current and voltage range that must be chosen to encompass the relevant behaviour of the solar cell. Figure 4 shows the resulting IV curves from Equation 3 for individual cells when the parameters are chosen as $V_d^t = 0.1135\,\mathrm{V}$, $I_d^{sat} = 10^{-10}\,\mathrm{A}$, $R_p = 400\,\Omega$, $R_s = 0.001\,\Omega$, $V_b^t = 0.03\,\mathrm{V}$, $I_b^{sat} = 10^{-3}\,\mathrm{A}$. It is assumed that $I_{pv} = 0.5009i\,\mathrm{A}$ where i is the illumination factor (in solar constants) of the individual cell being considered. These parameters were tuned by hand to approximate the output of the Azur Space 3G30A space-rated solar cells as given in the datasheet [18] after a radiation fluence of 10^{15} (1 MeV electrons/cm^2). The simulation window is set to $V_{rng} = [-0.4, 2.6]\,\mathrm{V}$ and $I_{rng} = [0, 0.6]\,\mathrm{A}$. The curve exhibits a "flat" region in which the last two terms of Equation 3 are negligible. When the applied voltage is increased, the first of these terms will grow exponentially and cause the sharp drop in output current. If the voltage is instead decreased, the last term will grow, causing the sharp increase in output current. The voltage in this region is negative, thus this corresponds to power lost in the cell.

Each series string of cells is often fitted with a series protection diode to prevent current from flowing in reverse and damaging the cells. Its characteristic is given by the diode equation:

$$I = I_{spd}^{sat}\left(\exp\left(-V/V_{spd}^t\right) - 1\right) \qquad (4)$$

Where I_{spd}^{sat} is the saturation current and V_{spd}^t the effective thermal voltage for the series protection diode. Assuming $I \geq 0$, Equation 4 can be inverted to read:

$$V = -V_{spd}^t \ln\left(I/I_{spd}^t + 1\right) \qquad (5)$$

The same parameter values as for the bypass diode were used in the implementation.

One should not be misled to believe that the parameters of space solar cells are constant. As the temperature of the solar cells varies throughout an orbit, the saturation currents and thermal voltages of all components will change. Higher temperatures will increase the current moderately but decrease the voltage a cell can support significantly. At an increase in temperature of 50°C above ambient, the maximum power is reduced by 14%[3] [18] for

[3]The maximum-power-point voltage decreases from 2.244 V to 1.884 V and the current increases from 0.4851 A to 0.4991 A.

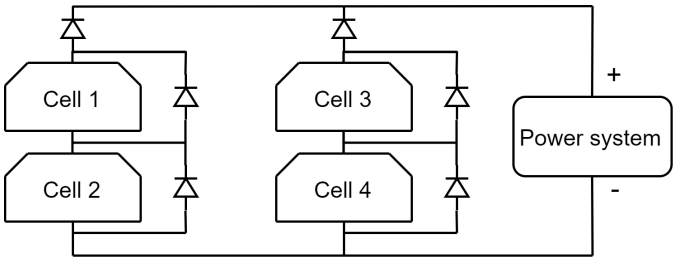

Figure 3: A panel connected as 2s2p.

the modelled cells. If the temperature profile in orbit is known, the modelling presented in this paper could be improved by introducing temperature dependence in Equation 3. In the long term, degradation of the solar cells due to the irradiation of charged particles will also decrease the power output [19].

2.2. Series and parallel connection modelling

Several approaches can be taken to finding the total IV curve of a solar panel of several cells. One such method that involves producing and numerically solving an equation system based on combining Equation 3 for each cell is given in [20]. In this work, an intuitive and simple to implement alternative method is presented. It relies on discrete sampling of the individual cell IV curves in a manner which will recover the corresponding series string IV curve at these samples. The result from this is combined by repeating a similar calculation to produce the full panel IV curve after the parallel connections.

For simplicity assume there are four cells on the satellite and these are connected in a $2s2p$ configuration as in Figure 3, where the illumination factors are respectively $i = \{1.0, 0.75, 0.5, 0.25\}$. Adapting the method to an arbitrary set of cells is straightforward. Denote the number of cells in series and parallel by $n_s = 2$ and $n_p = 2$. The cells are sampled with Equation 3 at N linearly spaced voltages in the set $\bar{V}_c \in V_{rng}$ and the corresponding currents produced at each cell are stored as $\bar{I}_c^{(1)}$, $\bar{I}_c^{(2)}$, $\bar{I}_c^{(3)}$, and $\bar{I}_c^{(4)}$. The IV curves and sample points for the case $N = 10$ are shown in Figure 4.

In each series string of the panel the same current must flow through each cell and bypass diode pair. Equation 3 gives the current as a function of voltage; the opposite is desired, so a numerical approach is taken. By deciding the currents to sample at, and using interpolation of the known cell IV curve, an approximation of the voltages across the cell is given at these currents. The *PCHIP* (Piecewise Cubic Hermite Interpolating Polynomial [21]) available in the standard distribution of *Matlab* is used in the implementation. Let the interpolated approximation of the voltage V at a current I based on the sample points $\{\bar{V}; \bar{I}\}$ be denoted as $V = \mathcal{P}\left(I \,|\, \{\bar{V}; \bar{I}\}\right)$.[4] Let $\bar{I}_s \in I_{rng}$ be a set of N

[4]I.e. $\mathcal{P}\left(I \,|\, \{\bar{V}; \bar{I}\}\right) = p(I)$ where p is the interpolating piecewise polynomial calculated with the points in $\{\bar{V}; \bar{I}\}$.

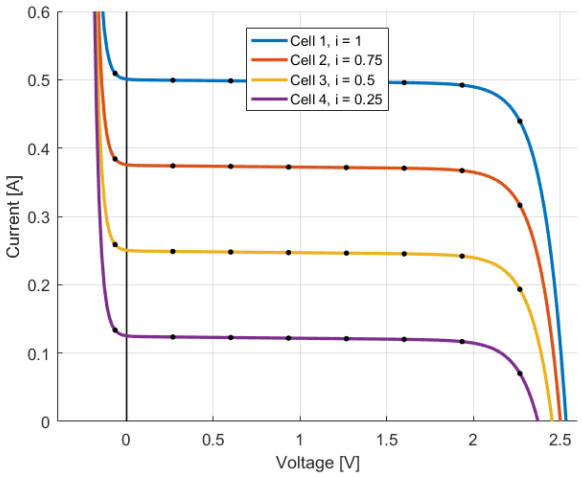

Figure 4: IV curve of individual cells at different illumination factors. Shown inside the simulation window and with sample points marked when $N = 10$. The current going to infinity at negative voltages is due to the bypass diode.

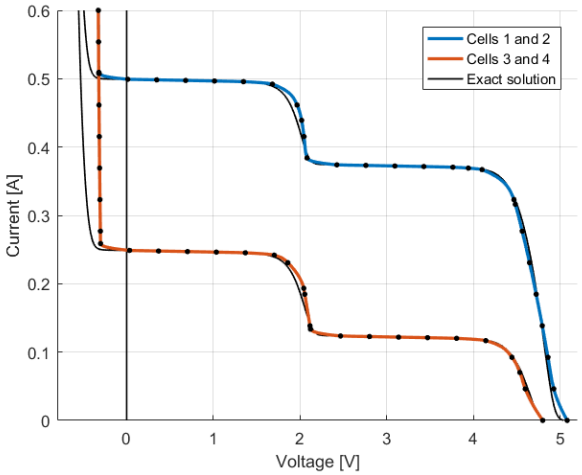

Figure 5: The sampled IV points for each of the series strings in the panel using $N = 10$. The curves connecting the sample points is given by *PCHIP* interpolation. The exact solution is given for large N, it is practically recovered when $N = 50$.

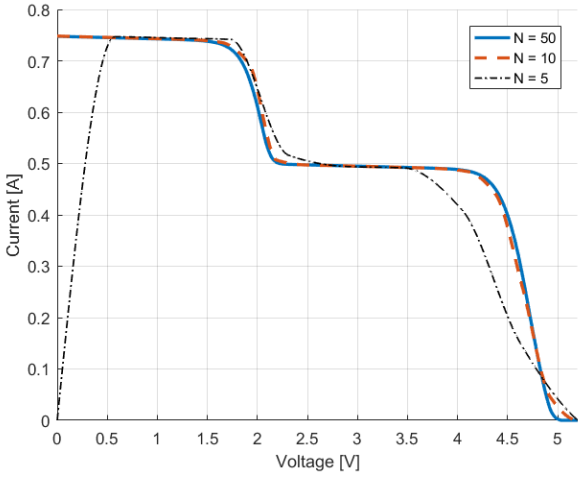

Figure 6: The combined panel output curve for the $2s2p$ panel of Figures 3-5. Several values of N are shown, the qualitative shape is preserved down to $N = 5$.

linearly spaced current points in the simulation window. If the sampling is carried out at only these points, a large number of samples N must be used to accurately approximate the IV curve of the series string since each cell's IV curve has a "flat" region where the current changes slowly. To combat this, a better choice of sampling points must be used. The individual cell sampling already provides a set of currents that will fall on each of these "flat" sections. By reusing these points together with the new sampling points a total of $(n_s + 1)N$ sampling points that are well spaced will be used. For the string with cells 1 and 2 specifically, the sampling currents and the interpolated voltages across the string becomes (where functions applied to sets are assumed element-wise):

$$\bar{I}_s^{(1,2)} = \bar{I}_c^{(1)} \cup \bar{I}_c^{(2)} \cup \bar{I}_s \tag{6}$$

$$\bar{V}_s^{(1,2)} = \sum_{j=1,2} \mathcal{P}\left(\bar{I}_s^{(1,2)} \,\middle|\, \{\bar{V}_c; \bar{I}_c^{(j)}\}\right) - V_{spd}^t \ln\left(\bar{I}_s^{(1,2)}/I_{spd}^t + 1\right) \tag{7}$$

In the case that the points in $\bar{I}_c^{(i)}$ are not unique, they will be supplemented by adding more new points in $\bar{I}_s$ such that the total always is $(n_s+1)N$ and unique. The resulting IV curves and sample points for both strings are shown in Figure 5. The process of adding the curves together can be visualised by looking in Figure 4 at the two curves being added. For a given current, the voltages must be summed. A distinct step in the middle is thus seen when the current is between the short-circuit currents of the two cells. The positive voltage of one cell (ca. +2.3 V) is added with the negative voltage for the other cell (ca. −.2 V). If the cells being added have a similar illumination the short circuit current will also be similar. This step is thus only seen if the cells are mismatched in illumination, most commonly due to cells being partially shaded.

Since these strings are connected in parallel the voltage across each string must be the same, and their currents are added. For the final result, negative voltages are of little use. A set of $2N$ linearly spaced voltage samples are defined, $\bar{V}_p \in [0, 5.2]$, where both the number of points and the upper voltage range has been scaled by n_s. The final IV curve of the whole panel is given by sampling again, this time for the currents:

$$\bar{I}_p = \sum_{j=(1,2),\,(3,4)} \mathcal{P}\left(\bar{V}_p \,\middle|\, \{\bar{I}_s^{(j)}; \bar{V}_s^{(j)}\}\right) \tag{8}$$

The final result will consist of $n_s N$ points. The resulting curve and sample points are shown in Figure 6 for the illustrated case of $N = 10$, as well as for $N = 5$ and $N = 50$. Visually, this is simply the addition of the currents of the two curves in Figure 5. Going beyond $N = 50$ shows no practical benefit and is the suggested sample count for this method.

A pseudocode implementation is given in Algorithm 1 and a *Matlab* implementation is freely available on the project GitHub [3]. Notation from the text is generally retained. For variables denoted with bars, the first dimension is omitted from the indexing.

Algorithm 1 Calculate total panel IV curve.
Input: array i, scalars n_s, n_p, N.

Require: Length$(i) = n_s n_p$
  $\bar{V}_c \leftarrow$ Init. N lin. spaced values in V_{rng}
  $\bar{V}_p \leftarrow$ Init. Nn_s lin. sp. values, 0 to $n_s \cdot V_{rng}[2]$
  $\bar{I}_p \leftarrow$ Init. Nn_s zeroes
  for $j = 1$ to $n_s n_p$ **do** *//Sample each cell*
    $\bar{I}_c[j] \leftarrow$ Eq. 3 with V=$\bar{V}_c$ and i=$i[j]$
  end for
  for $k = 1$ to n_p **do** *//Each series string*
    $a[1{:}n_s] \leftarrow (1 : n_s) + n_s(k-1)$ *//ind. in string*
    $\bar{I}_o \leftarrow$ unique vals. of $\bar{I}_c[j]$, inside I_{rng}, $\forall j \in a$
    $\bar{I}_n \leftarrow (n_s{+}1)N{-}\text{Len}(\bar{I}_o)$ lin. sp. values in I_{rng}
    $\bar{I}_s \leftarrow \bar{I}_o \cup \bar{I}_n$
    $\bar{V}_s \leftarrow$ Eq. 5 with I=$\bar{I}_s$
    for $l = 1$ to n_s **do** *//Each cell in string*
      $P \leftarrow interp.create(\bar{V}_c, \bar{I}_c[a[l]])$
      $\bar{V}_s \leftarrow \bar{V}_s + P.evaluate(\bar{I}_s)$
    end for
    $P \leftarrow interp.create(\bar{I}_s, \bar{V}_s)$
    $\bar{I}_p \leftarrow \bar{I}_p + P.evaluate(\bar{V}_p)$
  end for
  return $\bar{I}_p, \bar{V}_p$

3. Hardware simulator

3.1. Overview

A hardware simulation system (named the Solar Panel Simulator, SPS, Figure 7) was designed to emulate the solar panel behaviour (the IV curve) in orbit and apply this to the spacecraft power system. An analogue circuit (Figure 8) designed as a constant current source is connected to the satellite. With the relatively low power requirements, a linear design was chosen to simplify the circuit and provide low noise. This is in turn controlled by a digital feedback loop (Figure 9), running at 1 kHz. The hybrid design ensures that there is no switching noise even at this modest rate, and makes a low capacitance output possible. The digital circuit measures the output voltage (as applied by the satellite SAI) and sets the corresponding current from a lookup-table (LUT) to reproduce the desired IV curve. The board and circuit were designed for an input voltage between 12 and 24 volts. Due to the drop across the transistor, the maximum output voltage is approximately 3 V less than the input. The maximum power dissipation from the heatsink is 25 W. As most satellites have several independent inputs the system is intended to be used with several separate SPS boards, each simulating either one SAI input or one physical solar panel of the satellite. The design files and software related to the SPS are freely available on the project GitHub [3].

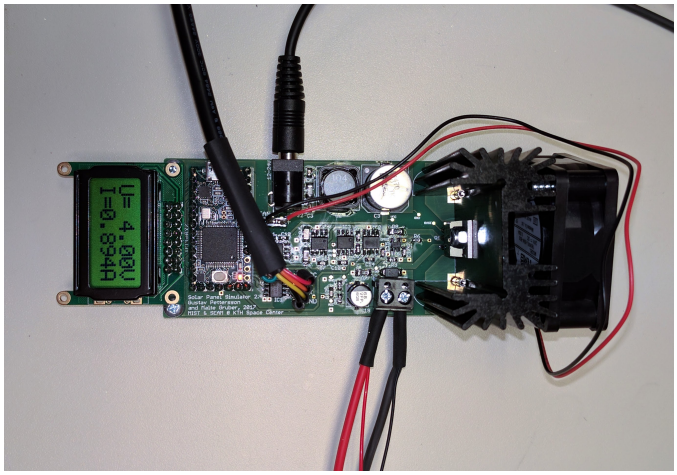

Figure 7: The assembled solar panel simulator PCB. The dimensions of the board are approximately 150 × 50 mm. The design files are freely available on the project GitHub [3].

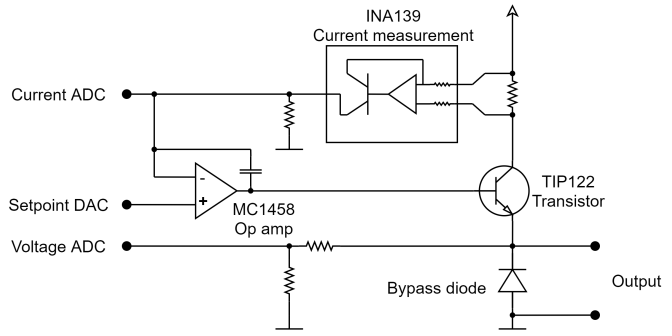

Figure 8: Simplified schematic of the analogue circuit. High-side current measurement is used in an op-amp feedback loop to follow the setpoint current. A capacitor placed across the op-amp provides lead compensation to ensure stability. The three connections to the microcontroller are on the left and the output to the satellite is on the right. The full schematic is freely available on the project GitHub [3].

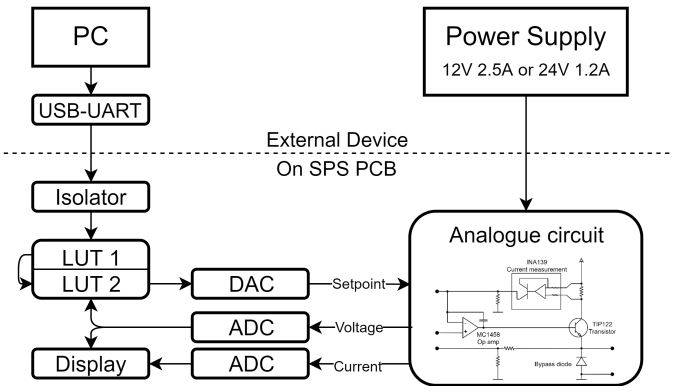

Figure 9: Flowchart overview of the digital system. A double buffer is used for the LUT and the board is isolated provided an isolated power supply is used.

3.2. Design

The SPS is designed as a cascade control system, where the current is controlled by an analogue feedback and the IV curve by digital feedback applied as input to the analogue circuit. The hardware is implemented on a PCB shown in Figure 7. A schematic of the analogue circuit is shown in Figure 8. The digital control is applied in a Teensy 3.2 microcontroller [22] through two 12 bit analogue-to-digital converters (ADCs), and one 12 bit digital-to-analogue converter (DAC), integrated in the Teensy 3.2. This microcontroller runs the digital feedback loop at 1 kHz, with which an arbitrary IV curve can be produced at the output. A flowchart of the digital system is shown in Figure 9. The curve is stored in a LUT which is updated by a computer over USB. A double buffer is implemented to store the LUT, where one array is used for writing a new LUT while a second array is used for reading the current LUT. The array from which the current IV curve is read (LUT 2) is only updated when the transfer is successfully completed; no interruptions or incomplete IV curves will be present at the output. The LUTs are stored as 16-bit arrays of length 4096, each requiring 8 kB of memory (however the values stored are only 12-bit). The computer connection is made over an isolated serial[5] connection. To transfer over this 8-bit protocol each value of the LUT is split into two, using the excess bits as identifiers. The value read from the DAC is used as the index in which to read from the LUT and the value stored is set to the ADC as the desired current. The voltage measurement and current setpoint are calibrated for each SPS with regards to their corresponding digital value and are stored as a pair of polynomials, in the PC, to generate the LUT for the device. The measured voltage and current at the SPS output (and thus SAI input) is shown on an LCD mounted on the board. The SPS has been designed to allow the outputs of several SPSs to be combined in either series or parallel connection if desired. This opens the possibility of using one SPS to simulate each physical solar panel on the CubeSat for easy integration into the wiring harness, or alternatively to provide more power for satellites with larger solar panels. Using 12 V input, the maximum output is 2.1 A at 8 V. Using 24 V input, the maximum output is 1.1 A at 21 V.

3.3. Testing

Since the SPS is designed as a cascaded control system, it is vital that the inner (analogue) feedback has a much greater bandwidth than the outer (digital) feedback. With this, the analogue feedback system can be treated as perfect (i.e. ignored) when the digital controller is designed [23]. In order to measure the bandwidth of the analogue circuit, a step change of the desired current was applied to the analogue circuit, as shown in Figure 10, while the

[5] A Universal Asynchronous Receiver-Transmitter (UART) link running at a rate of 115200 symbols/second.

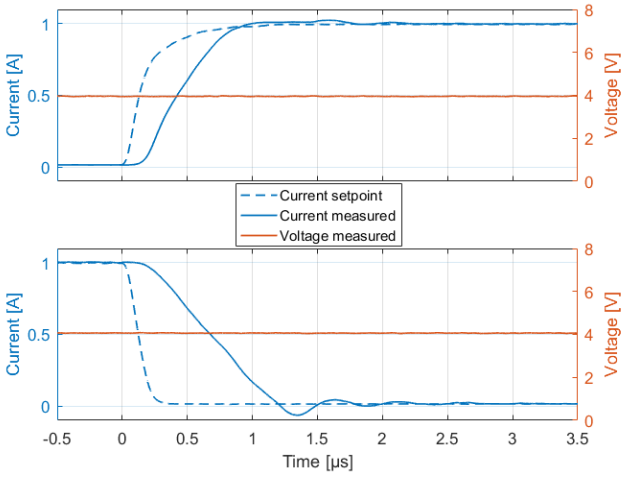

Figure 10: Rising and falling step response of the analogue circuit. The circuit was connected to a DC load in constant voltage mode. Shown as *setpoint* is the measured output of the DAC (scaled to current).

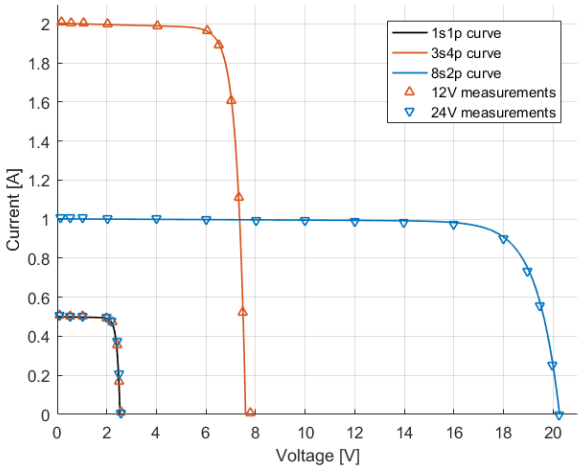

Figure 11: Testing of realistic IV curves for the SPS. Testing was completed using a DC load and multimeter in a four wire configuration. The voltages in the legend refer to the input voltage provided to the analogue circuit.

digital feedback was disabled. The measurements show a rise time of approximately 1 microsecond, corresponding to a bandwidth of over 300 kHz. The digital bandwidth is, due to the selected sampling rate, below 1 kHz. Thus the cascade controller design is valid and we shall turn to considering the combined analogue and digital system.

To test the accuracy of the output of the SPS, realistic solar panel curves were programmed into the SPS. The curves are based on scaling the $i = 1$ curve in Figure 4, by multiplying the voltage and current by an integer number of cells in series and parallel. To measure the output, a constant voltage DC load was connected to the output and a range of voltages tested. The results in Figure 11 show that the SPS is capable of accurately reproducing the desired currents and voltages for both small and large output powers.

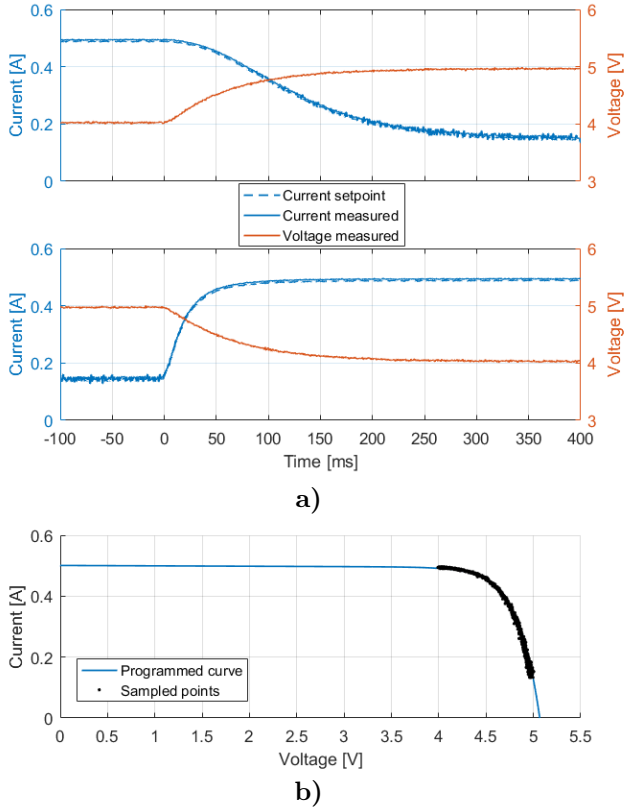

Figure 12: Dynamic response of the digital feedback system. A $2s1p$ LUT was applied to the system and the externally driven voltage was changed. **a)** Shows the current and voltage over time. **b)** Show a scatter plot of the measurements of **a)** on the programmed curve.

A dynamic test to confirm that the SPS correctly follows the desired IV curve when the applied voltage changes was conducted. The results in Figure 12 show that the SPS responds to the change in voltage smoothly and that the programmed IV curve is tracked throughout. The measurements show that the noise level of the SPS output is approximately ± 10 mV and ± 5 mA in voltage and current respectively. The response time in these measurements is limited by the speed of the DC load, and are not indicative of the SPS response time.

Finally, a real-world test was conducted where the SPS was connected to the SEAM [24] satellite, a 3U CubeSat powered by a Gomspace Nanopower P60 SAI. Figure 13 shows the curve which was programmed into the SPS together with a measurement of the output voltage over time. The voltage of this system is controlled by the Gomspace SAI by an MPPT technique. By comparing the applied voltage with the maximum power point in the applied curve, it is clear the SAI is successful in tracking.[6] The measurements also show that the SPS rise time is below 1 ms, allowing its use on faster SAIs as well.

[6]Some interesting inferences about the particular SAI can also be made; the update rate is 5 Hz and the voltage is controlled in steps of 50 mV.

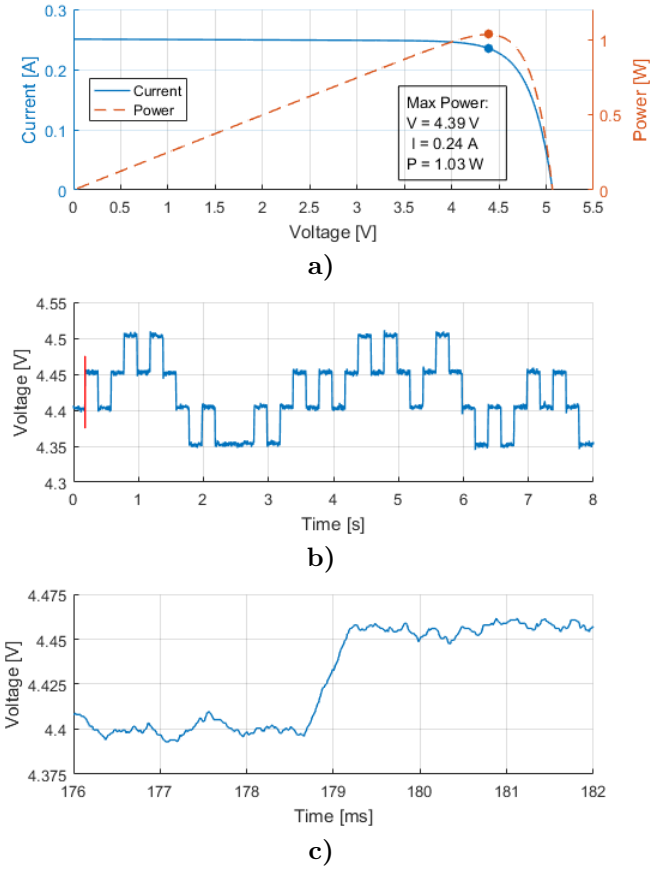

Figure 13: Testing the SPS connected to a CubeSat MPPT. **a)** Shows the IV curve programmed into the SPS and the corresponding PV curve and maximum power point. **b)** Shows a measurement over time of the output voltage applied by the Gomspace Nanopower P60 MPPT SAI. **c)** Shows an enlarged view of the region marked in red in **b)**, where the response time of the SPS is seen.

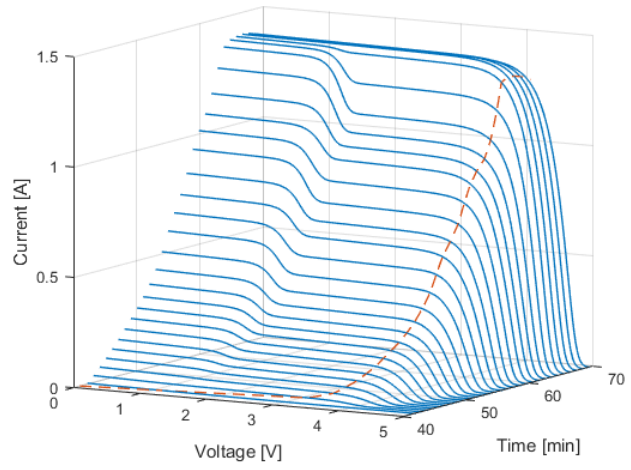

Figure 14: Evolution of IV curve (solid) at one SAI input. Data taken from a simulation of the MIST [25] satellite, showing approximately one third of an orbit at MPPT 2. The broken line shows the location of the maximum power point.

4. Real-time IV updating

As the satellite orbits, the solar incidence angle changes with time. This creates a dynamic situation, where the output of the solar panels is changing and hence the power available to the satellite. Figure 14 shows how the IV curve evolves during a nominal orbit and how the maximum power point also moves. This figure shows the complex evolution which can be seen in the real world. A significant step in the IV curve, caused by partial shading during parts of the orbit, is clearly visible. During less ideal circumstances, e.g. tumbling, the behaviour may change rapidly and cause issues for the SAI of the satellite.

To provide realistic input to the SAI for any desirable situation, software for real-time control of the SPS was created. It is assumed that the illumination factor for every cell is known, together with a timestamp. Using a real-time clock, the methods of Section 2 are applied to this data at the appropriate time, to provide the IV curve that should be present at each SAI or solar panel input of the satellite. These curves are converted, using the individual calibration polynomials, to unique LUTs for the SPSs that are connected to the corresponding inputs. These are then sent to the hardware devices over the USB connection as in Section 3. This system is agnostic to the input data. Hand calculated approximations of the illumination factors or complex simulations incorporating e.g. realistic attitudes, deployment failures, or tumbling, may all be used depending on the desired level of realism.

4.1. Demonstration

The purpose of this paper is to allow realistic real-time testing of the power systems on CubeSats. In Figure 15 a setup using three SPSs simultaneously to power each independent MPPT input on the MIST Gomspace Nanopower P31us is shown. In-house simulations of the solar conditions in orbit, including effects of self-shading, is used as the input data for this test. The test is run from a simple Graphical User Interface (GUI) where the simulation is controlled and the current state of the SPSs are displayed. This GUI, the underlying classes for controlling the SPSs via a computer, and a GUI for manual control of SPSs, are freely available on the project GitHub [3].

The results of running one orbit are shown in Figure 16. The SPSs are updated every 6 seconds with a new IV curve. The line shown in the figure is the maximum power point of the IV curve programmed in each SPS and how it evolves over the orbit. The housekeeping data from the SAI is sampled every 6 seconds and shown as the broken lines. The agreement between these values across the entire orbit shows that the MPPT system of the satellite is tracking the IV curves correctly, and is producing power as efficiently as possible. Since the SPSs have been shown in Figure 11 to be accurate, the difference seen between the curves is is likely due to measurement errors by the Gomspace P31us.

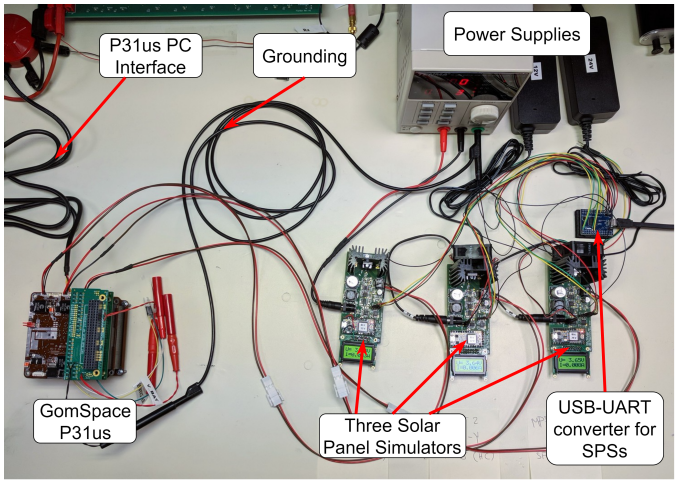

a)

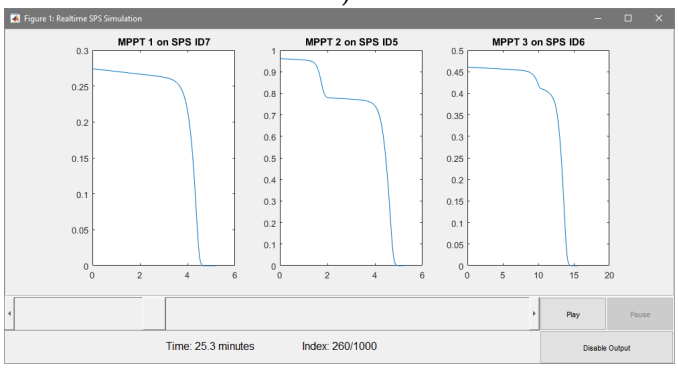

b)

Figure 15: Test setup with several SPSs running real-time updating. **a)** Shows the components and how they are connected. **b)** Shows the PC user interface with the current IV curves programmed in each SPS, a timeline, and user controls.

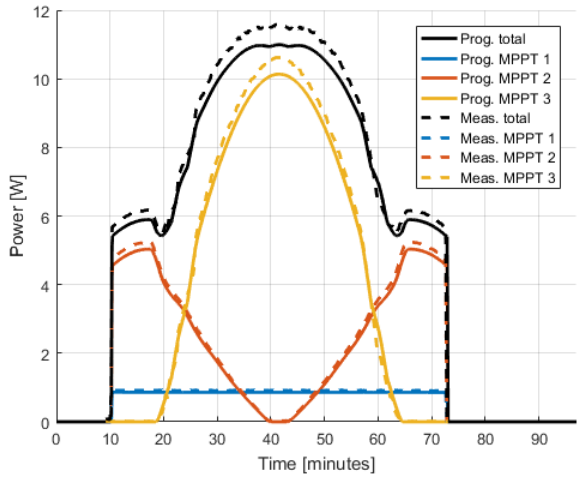

Figure 16: Real-time simulation of one orbit for the MIST satellite. The solid lines show the maximum power point of the programmed IV curves on each of the connected SPSs. The broken lines show the input powers as reported by the Gomspace P31us housekeeping data.

5. Conclusions

We have developed hardware (the SPS) and a methodology to provide realistic and accessible testing of the power system aboard nanosatellites. The hybrid approach to the SPS of combining an analogue constant current circuit with digital feedback provides a low noise output and avoids high-frequency digital feedback. The hardware can provide approximately 25 W of power and arbitrary, time-dependent, IV curves. We presented a methodology to generate realistic IV curves from knowledge of the illumination of the satellite solar cells. It relies on the previous development of models for assessing power generation in orbit and is intuitive and simple to implement. Any scenario for which the orbit solar conditions have been simulated can be applied with the system. The Solar Panel Simulator has been demonstrated to produce realistic outputs and real-time updating. Finally, the system has been released as Open Source in the hope that it will be useful for other nanosatellite developers as well. We invite discussion and collaboration on the project GitHub [3].

Acknowledgements

We thank the supporters of the SEAM and MIST satellites at KTH. The work on SEAM was funded through the European Union FP7 programme as project 607197. The work on MIST was funded through grants from the Knut and Alice Wallenberg Foundation and the ÅForsk Foundation. We thank our colleagues Nickolay Ivchenko and Agnes Gårdebäck for the fruitful discussions, as well as Marcus Ackland and Björn Ordoubadian for the editorial help.

References

[1] D. Y. Lee, J. W. Cutler, J. Mancewicz, A. J. Ridley, Maximizing Photovoltaic Power Generation of a Space-Dart Configured Satellite, Acta Astronautica 111 (2015) 283 – 299.

[2] R. Ramabadran, B. Mathur, Effect of Shading on Series and Parallel Connected Solar PV Modules, Modern Applied Science 3 (10) (2009) 32 – 41.

[3] G. M. Pettersson, M. Gruber, T.-A. Stana, S. Grahn, C. Fuglesang, Solar-Panel-Simulator repository, `github.com/gustavmpettersson/Solar-Panel-Simulator`, accessed: 15 Jan 2018.

[4] J. Bouwmeester, J. Guo, Survey of worldwide pico- and nanosatellite missions, distributions and subsystem technology, Acta Astronautica 67 (7) (2010) 854 – 862.

[5] D. Erb, S. Rawashdeh, J. Lumpp Jr, Evaluation of solar array peak power tracking technologies for cubesats, in: 25th Annual AIAA/USU Conference on Small Satellites, 2011.

[6] Gomspace NanoPower P31u, `gomspace.com/Shop/subsystems/power-supplies/nanopower-p31u.aspx`, accessed: 8 Sept 2017.

[7] H. Nagayoshi, S. Orio, Y. Kono, H. Nakajima, Novel PV array/module I-V curve simulator circuit, in: Conference Record of the 29th IEEE Photovoltaic Specialists Conference, 2002, pp. 1535–1538.
[8] J. Ollila, A medium power PV-array simulator with a robust control strategy, in: Proceedings of International Conference on Control Applications, 1995, pp. 40–45.
[9] E. Koutroulis, K. Kalaitzakis, V. Tzitzilonis, Development of an FPGA-based system for real-time simulation of photovoltaic modules, Microelectronics Journal 40 (7) (2009) 1094 – 1102.
[10] Y. Li, T. Lee, F. Z. Peng, D. Liu, A Hybrid Control Strategy for Photovoltaic Simulator, in: 24th Annual IEEE Applied Power Electronics Conference and Exposition, 2009, pp. 899–903.
[11] Keysight E4360 Modular Solar Array Simulators, `keysight.com/en/pc-1367756/e4360-modular-solar-array-simulators`, accessed: 8 Sept 2017.
[12] M. E. Bas, I. E. Akyol, M. S. Uludag, A. B. Ecevit, A. R. Aslan, Solar Emulator and Simulator Design for CubeSats, in: 63rd International Astronautical Congress, 2012.
[13] S. A. Rawashdeh, M. Simonds, J. E. Lumpp, V. Zeps, Solar Simulator for Spacecraft Photovoltaic Power System Hardware-in-the-Loop Testing, Journal of Small Satellites 5 (2) (2016) 457 – 466.
[14] A. R. Jordehi, Parameter estimation of solar photovoltaic (pv) cells: A review, Renewable and Sustainable Energy Reviews 61 (2016) 354 – 371.
[15] A. Jain, A. Kapoor, Exact analytical solutions of the parameters of real solar cells using Lambert W-function, Solar Energy Materials and Solar Cells 81 (2) (2004) 269 – 277.
[16] G. Segev, G. Mittelman, A. Kribus, Equivalent circuit models for triple-junction concentrator solar cells, Solar Energy Materials and Solar Cells 98 (2012) 57 – 65.
[17] A. B. Or, J. Appelbaum, Estimation of multijunction solar cell parameters, Progress in Photovoltaics: Research and Applications 21 (4) (2013) 713–723.
[18] Azur Space 30% Triple Junction GaAs Solar Cell Assembly, `azurspace.com/images/products/0003401-01-01_DB_3G30A.pdf`, accessed: 15 Jan 2018.
[19] S. Makham, M. Zazoui, G. C. Sun, J. C. Bourgoin, Non-empirical prediction of solar cell degradation in space, Semiconductor Science and Technology 20 (8) (2005) 699.
[20] G. Petrone, C. Ramos-Paja, Modeling of photovoltaic fields in mismatched conditions for energy yield evaluations, Electric Power Systems Research 81 (4) (2011) 1003 – 1013.
[21] F. N. Fritsch, R. E. Carlson, Monotone Piecewise Cubic Interpolation, SIAM Journal on Numerical Analysis 17 (2) (1980) 238–246.
[22] Teensy USB Development Board, `www.pjrc.com/teensy`, accessed: 10 Sept 2017.
[23] C. L. Smith, Cascade Control, John Wiley & Sons, Inc., 2010, pp. 38–85.
[24] Small Explorer for Advanced Missions, `fp7-seam.eu`, accessed: 8 Sept 2017.
[25] MIST - The Miniature Student Satellite, `mistsatellite.space`, accessed: 8 Sept 2017.

Author Biographies

Gustav M. Pettersson was born in Gothenburg, Sweden, in 1994. He received the B.Sc. in Engineering Physics from the KTH Royal Institute of Technology, Stockholm, in 2017. He is currently a M.Sc. student in Aerospace Engineering, also at KTH. He was a Summer Undergraduate Research Fellow at the California Institute of Technology, Pasadena, in 2016 and a Research Engineer at the Science for Life Laboratory, Solna, in 2017. He is currently an intern in the Intelligent Robotics Group at the NASA Ames Research Center, Moffett Field.

Malte Gruber was born in Södertälje, Sweden. He currently studies for the MSc degree in Embedded Systems at KTH Royal Institute of Technology. Since 2016 he has been a software developer for the SEAM satellite.

Theodor-Adrian Stana is an electrical engineer with the Particle and Astroparticle Physics group of the School of Engineering Sciences at KTH Royal Institute of Technology. Here, his work revolves around developing instrumentation for measuring X- and gamma-ray polarization. He is the supervisor of the electrical and functional testing teams of the MIST student satellite project, which are in charge of specifying, designing and testing the electrical interfaces between satellite sub-systems and experiments. Before his engineering activities at KTH, he was a fellow at CERN between 2012-2015; he earned an MSc at KTH in 2012 and a BSc at the Politehnica University of Timisoara, Romania, in 2010.

Sven Grahn is the project manager of the MIST student satellite at the KTH Space center. He has a MSc in Engineering Physics from KTH 1969. He has a long history of system engineering and management of major Swedish satellite projects over a period of forty years while he was employed by the Swedish Space Corporation. This includes Sweden's first satellite Viking and the first satellite entirely designed and built in Sweden, the 214 kg magnetospheric research satellite Freja, which was launched into orbit from China in 1992.

Christer Fuglesang is an astronaut and Professor at KTH Royal Institute of Technology and Director of KTH Space Center. His research mainly regards particles in space: radiation on the International Space Station and JEM-EUSO, a project studying ultra-high energy cosmic rays. In 2014 he initiated the MIST student satellite project. He has a MSc in Engineering Physics from KTH 1981 and a PhD in Particle Physics from Stockholm University 1987. He was a Fellow at CERN 1988-1990. In 1992 he became an ESA astronaut and made two space missions in 2006 and 2009.